Electronic Effects of Al Doping on the Mechanism of Methanol Formation on an Al Doped Cu/ZnO Interface Model

David A. Jurado A.,[a, b, c, d] Michael D. Higham,[c, d] C. Richard A. Catlow,*[c, d, e] and Ingo Krossing*[a, b]

The mechanism of CO_2 hydrogenation to methanol is modelled using plane-wave DFT applied to a representative Cu_8-ZnO(CZ) model, reported previously, with aluminium substituting a bulk Zn (= Cu/ZnO/Al_2O_3(CZA)). On CZA, CO_2 adsorption and activation are enhanced at the active Cu/ZnO interface compared to systems with a Cu-based or CZ-based interface, demonstrating Al's electronic effect. Methanol formation at CZA follows the formate path: $CO_2^*\rightarrow$ HCOO*$\rightarrow$ $H_2COO^*\rightarrow$ $H_2COOH^*\rightarrow$ $H_2CO^*\rightarrow$ $H_2COH^*\rightarrow$ H_3COH, with small contributions from the RWGS mechanism. Methoxy's binding is enhanced, making it a dead-end and not an intermediate as on CZ. Formate interme- diate at the Cu/Zn interface in CZA is electronically destabilized through Al. By contrast, other surface formates are stabilized and act as spectators. The most energy demanding step is the hydro- genation of formate to dioxomethylene ($E_a = 1.08$ eV) and not methoxy hydrogenation as on CZ. Multiple species are able to scavenge O* regenerating the active interfacial site. OH* was found to poison the active site, although its formation is energy demanding, making the CZA system overall more selective to MeOH than CZ. Water formation occurs on the Cu site as on the CZ system, although Zn sites can stabilize adsorbed water consistent to on experiments at CZA.

1. Introduction

The Cu/ZnO/Al_2O_3 (CZA) catalyst is applied to industrial methanol production via CO_2 hydrogenation and syngas conversion since the 1960s.[1–8] With rising atmospheric CO_2 lev- els, attributed to anthropogenic pollution,[9,10] it is anticipated that this process will be of growing importance,[11,12] coupled with sustainable photocatalytic water splitting[13–23] and carbon capture technology,[24–26] not only to alleviate CO_2 pollution, but also to develop a synthetic carbon cycle, parallel to nature's own,

to reduce dependence on fossil fuels and transition toward a sustainable circular economy.[27] As such, there is a considerable interest in the development of superior catalysts for methanol production, with rational catalyst design based on chemical and physical principles.

Despite the success of the industrial CZA catalyst, much remains poorly understood in terms of the role of each com- ponent, and how those components contribute to high activity, selectivity, and stability. It has been widely thought that Cu is the active phase, with ZnO stabilizing Cu(I) sites and Al_2O_3 provid- ing a stable substrate to prevent active particle sintering.[1,28–32] Although there is no doubt that these factors contribute to the observed catalytic behavior, it is also evident that the strong metal–support interaction between the Cu and ZnO phases,[33] and the electronic impact of the presence of Al, contribute to catalytic behavior in addition to these factors. The widely reported Cu/ZnO synergistic effect has been attributed to a number of factors, including maximizing Cu surface area,[34] the formation of active Cu/Zn alloy sites,[35] and the forma- tion of ZnO overlayers.[36] There have been extensive studies dedicated to investigate the nature of the interaction between the Cu and ZnO components, from both experimental[37–45] and theoretical[35,46–49] perspectives. However, the precise role of the alumina component has still not received as much attention.

In addition to its role as a structural promoter, Al_2O_3 was suggested to enhance catalytic activity via the presence of Al modifying the electronic properties of the catalyst surface, e.g., by stabilizing the active Cu^+ containing site, through hinder- ing the complete reduction of Cu^{2+} on Al_2O_3/ZnO interfaces with Cu rich clusters.[50] Indeed, promoting a Cu/ZnO cata- lyst with Al resulted in an increase in catalytic performance, although stability was suboptimal with Al segregation being observed.[51,52] The improved activity was also attributed to Al^{3+}

[a] D. A. Jurado A., I. Krossing
Institute for Inorganic and Analytical Chemistry, Albert-Ludwigs-Universität Freiburg, Albertstr. 21 D-79104, Freiburg, Germany
E-mail: krossing@uni-freiburg.de

[b] D. A. Jurado A., I. Krossing
Freiburg Materials Research Center FMF, Albert-Ludwigs-Universität Freiburg, Stefan-Meier-Str. 21 D-79104, Freiburg, Germany

[c] D. A. Jurado A., M. D. Higham, C. R. A. Catlow
Dept of Chemistry, University College London, 20 Gordon Street, London WC1H 0AJ, UK
E-mail: c.r.a.catlow@ucl.ac.uk

[d] D. A. Jurado A., M. D. Higham, C. R. A. Catlow
Research Complex at Harwell, Rutherford Appleton Laboratory, Oxon OX11 0FA, UK

[e] C. R. A. Catlow
School of Chemistry, Cardiff University, Main Building, Park Place, Cardiff CF10 3AT, UK

doping into the ZnO lattice, essentially facilitating n-type semiconducting behavior. Notably, also the reverse water–gas shift (RWGS) activity is correlated with free charge carrier concentration and easy charge transfer facilitating CO_2 activation.[48,53,54] However, while there is clear evidence for the electronic promotional effect on CO_2 hydrogenation activity, the impact of Al on the wider reaction mechanism for CO_2 hydrogenation to methanol is uncertain.

Hence, this work aims to determine the mechanistic route for methanol formation on a model catalyst surface that affords a more representative structural description of the CZA catalyst system and by applying plane-wave DFT calculations to investigate the competing reaction pathways. The robust CZA model is devised from previous studies on the Cu/ZnO (CZ) system.[55–57] Using our recent mechanistic study of the competing reaction pathways for methanol formation on this model CZ surface as a benchmark,[58] the present work demonstrates how even very dilute concentrations of Al can have an impact on the most favorable reaction mechanism, in some cases significantly, and in other cases more subtly. The calculations allow us to rationalize spectroscopic observations of dominant surface species, which can be assigned as intermediates, spectators, or poisons, depending on their stabilities and the kinetic feasibility of processes producing or consuming those species. The work thus provides valuable insights into the activity of the industrial CZA catalyst, as well as identifying challenges and limiting factors to be addressed in the development of the next generation of methanol catalysts.

2. Methodology

2.1. Periodic Ab Initio Calculations

All periodic DFT calculations were performed using the Vienna Ab-initio Simulation Package (VASP).[59–62] The electronic structure was calculated using the projector augmented wave (PAW) approximation for the core-valence interactions, and the Perdew–Burke–Ernzerhof for solids (PBE_{Sol}) exchange-correlation functional was used throughout.[63–65] Our earlier work demonstrated that periodic plane-wave DFT using the PBE_{SOL} functional as implemented in *VASP*, in comparison with "gold standard" coupled cluster calculations, reproduced the trends in total energy for all relevant isolated molecular and intermediate species, thus demonstrating the suitability of this approach for modelling heterogeneous catalyst systems.[58] The plane wave cut-off was set at 450 eV, which was determined to be sufficient from previous studies[57,66] with further testing using a 700 eV cut-off in our previous report showing no appreciable difference in adsorption energies. All calculations were performed using a single Γ-centred k-point, owing to the large size of the cell.

Our model was obtained following several previous investigations.[57,67–70] The slab model consists of a 5×5 Zn-rich O-terminated reconstructed polar ZnO surface supercell, representing the support, on which a Cu_8 cluster is adsorbed. The structure is illustrated in Figure 1. The ZnO support slab consists of six ZnO layers, corresponding to a pristine, unreconstructed

O-terminated ZnO(0001) 5-layer slab, with the 6th layer being formed by an optimized array of Zn adatoms. An equal number of randomly selected Zn atoms on the opposing termination were removed to ensure overall charge compensation, in line with the previous studies.[55] The slabs are separated by 18 Å of vacuum. All Cu atomic positions and the top 3 ZnO layers were allowed to relax during structural optimization until atomic forces were converged to within 0.01 eV Å^{-1}. The bottom three layers were fixed at their bulk positions. To account for the presence of alumina, a single bulk-like Zn atom was substituted for Al (atom #48 in model) to produce the model for the CZA system, reflecting structures reported in the literature, from both experiments and simulations.[71,72] All images of the surface were generated using the software VESTA[73] with images of atoms using the radii: H 0.46, C 0.77, O 0.74, Zn 1.37, Al 1.43, and Cu 1.28 Å. All electron density difference volumes used an isosurface level of 0.002 a_0^{-3}. Further methodological details for the density of states (DOS) calculations are presented in the Supporting Information.

The adsorption energies E_{ads} are calculated according to the following expression:

$$E_{ads} = E_{X-CuZnOAl} - E_{CuZnOAl} - E_{X(g)} \tag{1}$$

where E_{ads} refers to the adsorption energy of species X* on the surface, $E_{X-CuZnOAl}$ to the energy of the Cu_8@ZnO-Al surface with adsorbed X* on one specific site, $E_{CuZnOAl}$ the energy of the clean Cu_8@ZnO-Al surface, and E_X the energy of an isolated X molecule in the gas phase. Adsorbed species include H_2, CO_2, H_2CO, H_2O, HCOOH, and more.

Zero-point energy (ZPE) corrections were applied to all surface intermediates, transition states, and gas phase species, associated with formation paths for methanol synthesis. However, uncorrected values, which are usually reported in the literature,[42,74–78] are also provided in the Supporting Information to this work.

Vibrational normal modes were also calculated for the species relevant to the formation of MeOH, in order to provide a benchmark and to inform future experimental studies. Their vibrational frequencies were obtained using the finite displacement method and the harmonic approximation as implemented in the VASP code; all surface adsorbate atoms were displaced along with the coordinating atoms of the CZA surface. The species are classified as resting states (i.e., spectators or mechanistic "dead ends" for methanol formation), intermediates, and species that the calculations suggest are unlikely to be formed in appreciable concentrations on the surface. These results are reported in the Supporting Information.

3. Results and Discussion

Our results represent a natural continuation of those recently published by us on the CZ system.[58] As such, we will refer to these previous investigations, in order to make a direct comparison between the reaction mechanisms where aluminium is both absent and present, and thus establish the potential role
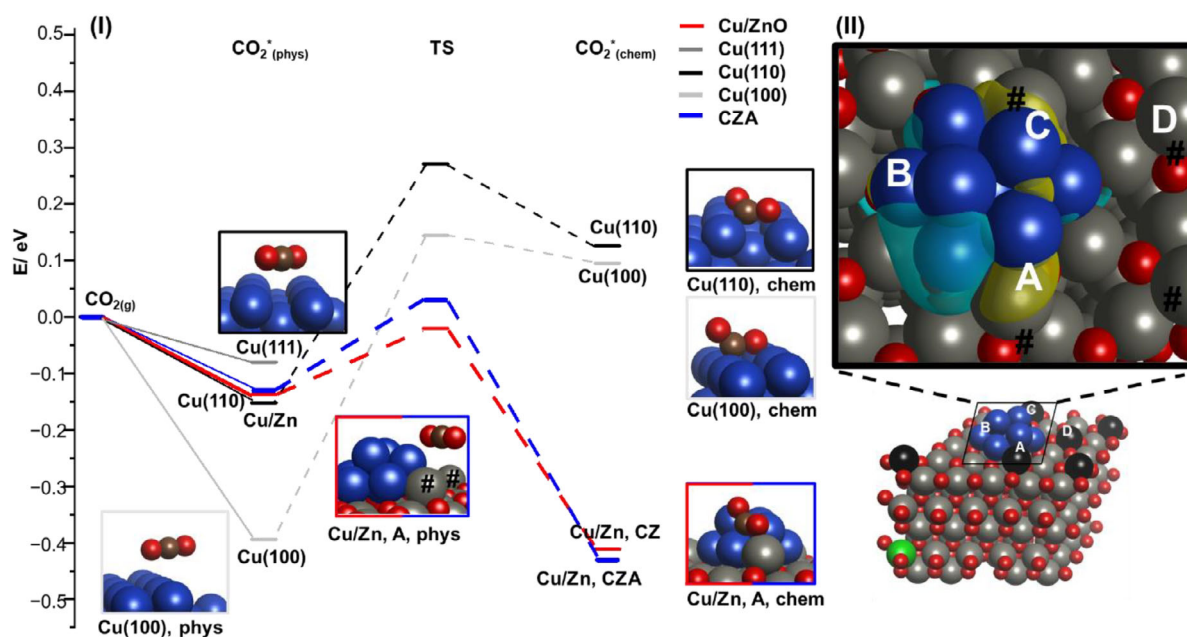
ChemCatChem

Research Article
doi.org/10.1002/cctc.202500824

Chemistry Europe
European Chemical
Societies Publishing

Figure 1. (I) Reaction profile illustrating ZPE corrected adsorption energies from physisorbed and chemisorbed CO_2 on different systems: the Al doped Cu/ZnO model system (CZA), the CZ system (CZ), and unsupported Cu.[69,81] At the interfacial site (A) of the CZ and CZA systems the adsorption of CO_2 is highly exothermic. Grabow et al.[81] reported in Cu(111) **no** chemisorption of CO_2, and suggested no need of it as formate would be formed through carbonate dissociation. We reported the importance of $CO_{2,chem}$ in our last publication,[58] and we emphasize that its vibrational modes lay in the same range as carbonate, suggesting an explanation to the carbonate band reported in the literature and a possible confusion of bands (Table S11 and Table S12). (II) Electron density isosurface difference plot of the surface of the doped model system CZA. Yellow regions denote an increase in electron density in comparison with bulk ZnO and the Cu cluster, teal regions a decrease. The increase in local charge density at the Cu/ZnO interface (A) of CZA is evident. Note that the teal region is closer to the A site in the CZA rather than the CZ analysis (Supporting Information).

of dilute aluminium in the electronic promotion of the CZ system. Notably, the presence of just one aluminium atom in the bulk layers of the slab model has an impact on the electronic structure of CZ and influences activation processes. This electronic influence is evident in the differences between the DOS for CZ and CZA shown in Figure S2 (Supporting Information)[79,80] and the impact of aluminium on the charge density localization at the surface as shown in Figure 1 (II) and in Figure S2, (Supporting Information). Additionally, aluminium enhances the concentration of conduction band electrons, which can help CO_2 activation.[48]

3.1. CO_2 Adsorption and Activation

The conversion of CO_2 to methanol necessarily requires the adsorption, and activation, of CO_2. On the Cu/ZnO interfacial site of the CZ system CO_2 adsorption is enhanced, compared to unsupported low-index Cu surfaces.[69,81] The impact of the presence of Al in the CZA system on CO_2 adsorption is summarized in Figure 1, and will be discussed in the following section.

In common with the CZ surface, CO_2 adsorption is enhanced at the Cu/ZnO interface site (A) of CZA, as well as at the Cu (B) and Zn site (D) (sites as defined in Figure 1). Although the energetics of adsorption of CO_2 on the CZ and CZA surfaces are very similar, there are differences in terms of the electronic and geometric structure of the adsorbed, activated CO_2 species (Table 1). Hence, the binding on the pure Cu site (B) is slightly more exothermic for the CZA system. Bader charge analysis (BCA) con-

versely suggests that for CZA, CO_2 chemisorbed on site (B) is less reduced, i.e., only by $0.33e^-$ versus $0.65e^-$ for the CZ system, while it is enhanced for the interfacial site. Note also that the O—C—O bond angle θ changes due to its stability or electron donation/acceptance, which is mainly due to partial CO_2 reduction being enhanced by partial filling of the antibonding π^* orbital, resulting in a narrower θ bond angle (Table 1).

The calculations also show that CO_2 chemisorption is feasible at the Cu (B), although partial CO_2 reduction is less pronounced at this site compared to the interfacial (A) site (E_{ads}, BCA and structural parameters Table 1).[68,82] In fact, this highlights the importance of the interfacial site (A): Although CO_2 can adsorb exothermically on all sites, only through its activation at the site (A), CO_2 undergo subsequent reaction processes toward methanol.[6,74,83–85] The very favorable adsorption at the Zn site (D) is remarkable and resembles the formation of a carbonate like species (cf. Supporting Information, Table S4). Note that the vibrational signature of chemisorbed CO_2 on the A site is in the same range as that of carbonate (cf. Supporting Information, Tables S11 and S12), which is visible by spectroscopic measurements.[86–91]

3.2. Further Reaction Progress Toward Methanol Formation

Following CO_2 adsorption and activation, the RWGS mechanism relies on the subsequent dissociation of CO_2. For this process, the CZ and CZA systems exhibit comparable behavior, with relatively high activation barriers of ~0.9 eV for CO_2 dissociation yielding

ChemCatChem

Research Article
doi.org/10.1002/cctc.202500824

Chemistry
Europe
European Chemical
Societies Publishing

Table 1. Adsorption energy, structural, and electronic parameters of the CO_2-moiety chemisorbed at the sites A, B, C, and D as calculated for the CZ (regular values) and the CZA (bold values) systems. CO_2 chemisorption energy E_{ads}, O—C—O bond angle θ, adsorbate Bader charge accumulation (β_X) in comparison to $CO_{2(g)}$ and bond lengths $d_{C\text{-}O\ (M)}$ and $d_{C/O\text{-}M}$ of chemisorbed CO_2. One of the O-atoms is closer to a Zn or a Cu atom, so to differentiate C—O lengths nearer to M (Zn or Cu).

| Site/from Figure 1	$E_{ads(chem)}$	$\theta/$ °	β_{CO2}	$d_{C\text{-}O(M)}$/Å	$d_{C\text{-}O(Cu)}$/Å	$d_{Cu\text{-}C}$/Å	$d_{M\text{-}O}$/Å
Interfacial A	−0.41/ **−0.43**	123.0/ **119.5**	0.77/ **0.87**	1.31/ **1.31** (M = Zn)	1.27/ **1.27**	1.94/ **1.93**	1.96/ **1.89** (M = Zn)
Top B	−0.36/ **−0.46**	133.4/ **132.8**	0.65/ **0.33**	1.30/ **1.30** (M = Cu)	1.22/ **1.22**	2.04/ **2.04**	2.04/ **2.03** (M = Cu)
Side C	−0.12/ **−0.07**	149.6/ **148.1**	0.36/ **0.37**	1.20/ **1.20** (M = Zn)	1.23/ **1.23**	2.16/ **2.17**	2.04/ **2.03** (M = Cu)
Zn D	−0.85/ **−0.88**	122.8/ **127.8**	0.34/ **0.39**	1.28/ **1.28** (M = Zn)	1.27/ **1.28** (Zn)	1.38[*]/ **1.38**[*]	2.04, 2.06/ **2.03, 2.06** (Zn)

[*] C—O bond, O from the surface ZnO.

CO at the interfacial site A (process [3]), and with the reaction being moderately endothermic for both systems, with CZ being slightly preferable. As a consequence, the RWGS-path via CO_2^* dissociation and subsequent hydrogenation of CO* (slow and endothermic, process [4]) is less competitive against direct CO_2 hydrogenation or CO_2 desorption. However, for the CZA system the subsequent hydrogenation of HCOO to H_2COO^* was found to be more energy demanding, making the possibility of the RWGS mechanism contributing to methanol formation more likely. In this path, CO_2 dissociation is followed by the subsequent hydrogenation of CO^*_A to HCO* and then to H_2CO^*, both low activation barriers. The calculations suggest that the possibility of methanol formation via the RWGS pathway is slightly enhanced for the CZA system in accordance to the literature,[79,92] since, as noted, the activation barrier for HCOO* formation is higher on CZA compared to CZ (process [14], 0.23 versus 0.00 eV), as is the activation barrier for subsequent HCOO hydrogenation (1.08 versus 0.93 eV for CZA versus CZ respectively), making CO_2^* dissociation more probable for the CZA rather than the CZ system.

3.3. The Most Favorable Mechanistic Path for Methanol Formation

Figure 2 shows the various overlapping mechanistic pathways and our proposal for the most favorable path for methanol synthesis. Table 2 then summarizes the calculated reaction energies for all the elementary processes investigated on the interfacial site of the CZA system, along with the corresponding activation barriers and imaginary frequencies for the unstable modes. The related data are also provided for the earlier calculated CZ interfacial site for comparison.

Overall, the calculations suggest that methanol formation will largely take place via the formate pathway, but will likely not proceed via the MeO* intermediate (as indicated by the bold red and black arrows in Figure 2):

$$CO_2* \rightarrow HCOO* \rightarrow H_2COO* \rightarrow H_2COOH* \rightarrow H_2CO*$$

$$\rightarrow H_2COH* \rightarrow H_3COH*$$
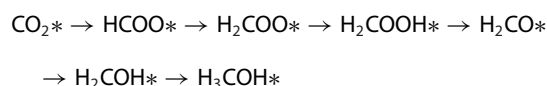
This sequence is similar to those previously reported for methanol formation.[75,86,87,93] However, in contrast to the CZ system, the activation barrier for methoxy hydrogenation is ~0.5 eV higher (due to the differences in stability of the initial and final states, *cf.* next section), as the process is substantially more demanding on the CZA model ($E_a = 1.55$ eV; $\Delta E = 1.13$ eV) than on CZ, which will hinder its consumption to yield methanol. Thus, it may well act as a spectator species, as suggested by the vibrations observed in experimental DRIFTS studies,[81,90,94–97] rather than an intermediate. Conversely, for CZA, the H_2COH^* intermediate yields a more competitive pathway for methanol formation. Although the formation of H_2COH^* via formaldehyde hydrogenation [7] has a higher barrier than methoxy formation for both CZA and CZ ($E_a = 1.00$ eV for CZA, $E_a = 0.94$ eV for CZ), H_2COH^* formation is modestly endothermic for CZA, but considerably more endothermic for CZ ($\Delta E = +0.19$ eV for CZA, $\Delta E = +0.49$ eV for CZ). In addition, the activation barrier for H_2COH^* hydrogenation to methanol [12] is considerably lower for CZA compared to CZ ($E_a = 0.66$ eV for CZ versus 0.57 eV for CZA), and the process energy is more exothermic for the CZA system ($\Delta E = −0.35$ eV for CZA versus $\Delta E = −0.26$ eV for CZ). Hence, the presence of aluminium favors methanol formation via the H_2COH^* intermediate, by both destabilizing the methoxy intermediate such that reverting to formaldehyde is competitive against the much slower hydrogenation to methanol, and by lowering the activation barrier for H_2COH^* hydrogenation.

Although the calculations suggest that formate creation may outcompete CO_2 dissociation and the mechanistic path for CO hydrogenation presents a less energy-demanding way to form H_2CO^*. It is the initial CO_2 dissociation (CO_2 scission, process [3]) that presents a challenge. Previous works employing empirical corrections especially for CO,[81,98] suggest that CO_2 dissociation is more favorable than ZPE corrected DFT calculations might suggest (without empirical values, this work), although the impact on other surface species remains unclear. This competing path is highlighted in Figure 3 in neon green (CZ) and teal (CZA) and also in Figure 2 with half-bold violet arrows. Hence, comparable trends in activation barriers and process energies are seen for both the CZ and CZA systems, although there are a number of key differences that are likely to have an impact
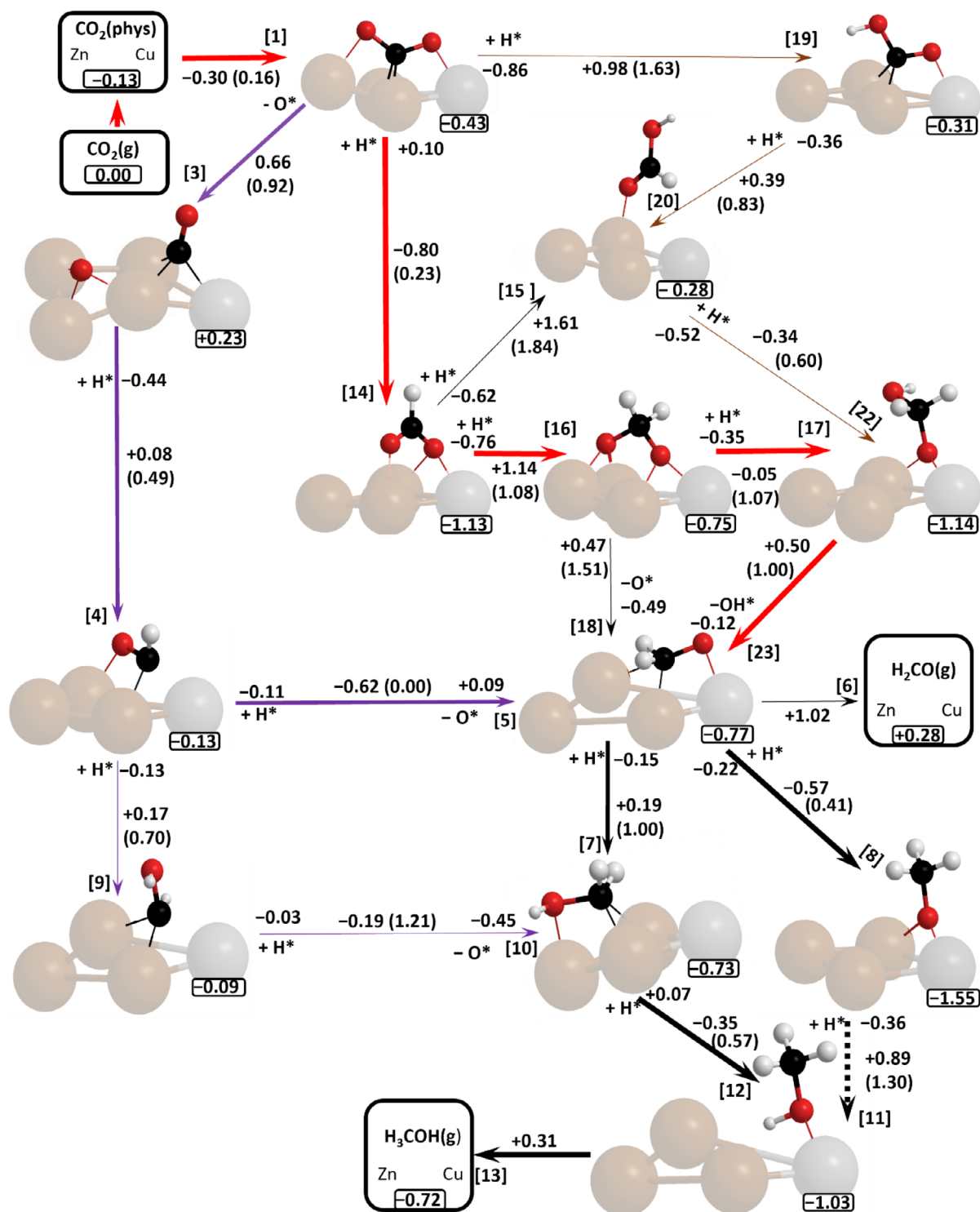
ChemCatChem

Research Article
doi.org/10.1002/cctc.202500824

Chemistry Europe
European Chemical
Societies Publishing

Figure 2. Simplified scheme of possible reaction pathways for methanol synthesis beginning with CO_2 on the interfacial site of the CZA system and as reported in our last publication.[58] For clarity, only processes involving C-containing species are shown. Process numbers [X] ($X = 1$–23), the respective reaction energy $\Delta_r E$ with its activation energy in parentheses (E_a) are given adjacent to each arrow. Energies of every species with respect to the gaseous reactants are listed in the black boxes (bottom right position of every adsorbate) and have been corrected with the ZPE of each species. The violet arrows are related to the RWGS path, brown for the COOH path and red for the formate path. The most favorable pathway (mix of formate and carboxyl) is indicated by bold arrows, but also the RWGS path seems to have an impact on the overall MeOH formation as indicated by half-bold arrows. The bold dashed line (process [11]) is a process that is difficult to occur and is one key difference to the CZ system. Details for all processes are listed in Table 2. The same image without the ZPE can be found in the Supporting Information of this article (Figure S3).

ChemCatChem

Research Article
doi.org/10.1002/cctc.202500824

Chemistry Europe
European Chemical
Societies Publishing

Table 2. Elementary processes described during the methanol formation on the interfacial site CZA and CZ for comparison and corrected with the ZPE. Each process number in the first column is related to an elementary process.

Step	Elementary process	E_a/eV	CZA ΔE/eV	E_a/ eV	CZ ΔE/eV
	Formate pathway related				
	CO_2 adsorption				
	$CO_{2(g)} \rightarrow CO_{2(phys)}$	–	−0.136	–	−0.137
[1]	$CO_{2(phys)} \rightarrow CO_2*$	0.157	−0.296	0.122	−0.274
	Formate and dioxymethylene formation				
[14]	$CO_2* + H* \rightarrow HCOO*$	0.232	−0.802	−0.050	−1.056
[16]	$HCOO* + H* \rightarrow H_2COO*$	1.079	+1.139	0.932	+1.007
	Formation and dissociation of H_2COOH*				
[17]	$H_2COO* + H* \rightarrow H_2COOH*$	1.067	−0.047	0.936	−0.007
[23]	$H_2COOH* \rightarrow H_2CO* + OH*$	1.004	+0.496	1.000	+0.639
[44]	$H_2COOH* \rightarrow H_2COH* + O*$	2.098	+1.361	2.250	+1.536
	H_2CO desorption				
[6]	$H_2CO* \rightarrow H_2CO (g)$	–	+1.385	–	+1.162
[8]	$H_2CO* + H* \rightarrow H_3CO*$	0.412	−0.567	0.141	−1.006
	Formation of methanol, desorption				
[11]	$H_3CO* + H* \rightarrow H_3COH*$	1.300	+0.890	1.086	+0.772
[13]	$H_3COH* \rightarrow H_3COH_{(g)}$	–	+0.311	–	+0.478
	Dissociations				
[18]	$H_2COO* \rightarrow H_2CO*_A + O*$	1.514	+0.466	1.394	+0.309
[28]	$HCOO* \rightarrow HCO*_A + O*$	1.808	+0.930	1.867	+0.934
[33]	$H_3COH* \rightarrow CH_3*_A + OH*$	1.579	−0.727	1.904	−0.758
	HCOOH-path, dissociation				
[15]	$HCOO* + H* \rightarrow HCOOH_{(phys)}$	1.837	+1.610	1.597	+1.305
[21]	$HCOOH* \rightarrow HCOOH_{(g)}$	–	+0.410	–	+0.353
[22]	$HCOOH_{(phys)} + H* \rightarrow H_2COOH*$	0.601	−0.344	0.484	−0.290
[35]	$HCOOH* \rightarrow HCO*_A + OH*$	0.581	−0.398	0.914	−0.359
[45]	$HCOOH* \rightarrow HCOH*_A + O*$	1.579	−0.081	1.723	+0.075
	Carboxyl formation, dissociation, and hydrogenation				
[19]	$CO_2* + H* \rightarrow Cu\text{-}COOH$	1.634	+0.983	1.626	+0.742
[20]	$Cu\text{-}COOH* + H* \rightarrow HCOOH_{(phys)}$	0.825	+0.387	0.867	+0.321
[27]	$Cu\text{-}COOH* \rightarrow CO* + OH*$	0.438	−0.026	0.600	−0.013
	H_2COH to methanol				
[7]	$H_2CO* + H* \rightarrow H_2COH *$	0.998	+0.171	0.940	+0.493
[12]	$H_2COH* + H* \rightarrow H_3COH*$	0.568	−0.354	0.657	−0.255
	RWGS related				
	CO_2 dissociation, CO hydrogenation				
[3]	$CO_2* \rightarrow CO*_A + O*_B$	0.924	+0.658	0.881	+0.583
[3-II]	$CO_2* \rightarrow CO*_B + O*_A$	0.310	−0.126	0.338	−0.262
[4]	$CO* + H* \rightarrow HCO*$	0.488	+0.078	0.527	+0.199
[29]	$CO* + H* \rightarrow COH*$	1.987[§]	+1.422	1.873[§]	+1.206
[34]	$CO* \rightarrow CO_{(g)}$		+0.679		+0.876
	Formaldehyde formation				
[5]	$HCO* + H* \rightarrow H_2CO*$	0.000	−0.620	0.610	−0.602

ChemCatChem

Research Article
doi.org/10.1002/cctc.202500824

Chemistry
Europe
European Chemical
Societies Publishing

| Table 2. (Continued)					
	Formaldehyde formation				
	HCOH formation and dehydrogenation				
[9]	HCO* + H* → HCOH*	0.701	+0.168	0.252	−0.221
[10]	HCOH* + H* → H$_2$COH*	1.210	−0.204	1.171	−0.090
[36]	COH* + H* → HCOH*	0.715	+0.043	0.793	+0.129
	Water processes				
[2]	$\frac{1}{2}$ H$_2$ → H*	–	−0.556	–	−0.700
[24]	O*$_A$ + H*$_B$ → OH*$_A$	1.079	−0.295	0.789	−0.659
[25]	OH*$_A$ + H*$_B$ → H$_2$O*	1.514	+0.683	1.337	+0.895
[26]	H$_2$O* → H$_2$O$_{(g)}$	–	+0.457	–	+0.483
[25B]	OH*$_B$ + H*$_B$ → H$_2$O*$_B$	0.841	+0.234	0.906	+0.227
	O/OH scavenging of A site				
[37]	O*$_A$ + HCO*$_B$ → HCOO*$_A$	0.595	−0.940	0.548	−1.047
[38]	O*$_A$ + H$_2$CO*$_B$ → H$_2$COO$_A$ *	0.043	−0.363	0.056	−0.333
[39]	O*$_A$ + HCOH*$_B$ → HCOOH*$_A$	0.632	−0.552	0.692	−0.630
[40]	O*$_A$ + H$_2$COH*$_B$ → H$_2$COOH*$_A$	1.119	−0.395	1.158	−0.319
[41]	OH*$_A$ + CO*$_B$ → COOH*$_A$	1.030	+1.071	1.111	+1.170
[42]	OH*$_A$ + HCO*$_B$ → HCOOH*$_A$	0.745	+0.588	0.673	+0.343
[43]	OH*$_A$ + H$_2$CO*$_B$ → H$_2$COOH*$_A$	1.073	+0.408	1.164	+0.537
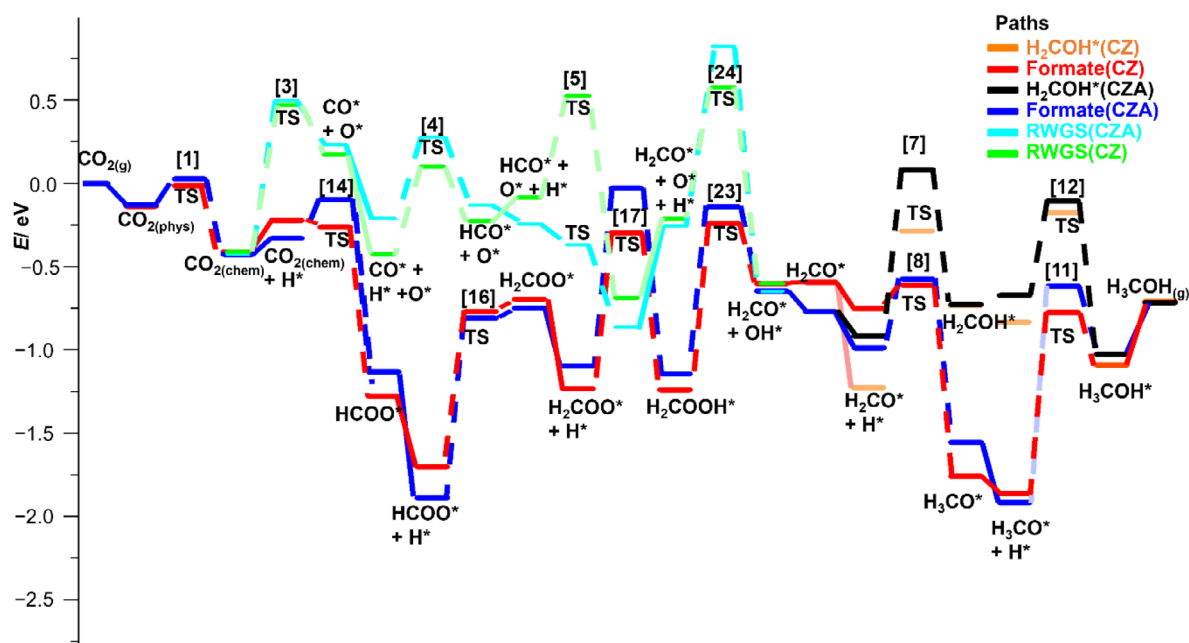
Figure 3. Reaction profile illustrating the formation of methanol via the less energy demanding formate-path (red and blue) and the alternative RWGS path (green and teal) on the CZ and CZA systems. Other intermediates are omitted; their corresponding energies are included in the SupportingInformation Transition states (TS) relate to dashed lines and process numbers from Table 2 are shown in brackets. Hydrogenation of formaldehyde leads to H$_3$CO* and H$_2$COH* (in orange and black) for CZ and CZA. Both may form, however, H$_3$CO* shows great stability on both CZ and CZA, but on CZA the H$_2$COH* route seems to be preferred to form MeOH on the surface. The dissociation of CO$_2$* (process[3]) and subsequently hydrogenation of CO* (to HCO*, then H$_2$CO*) have also an impact in the overall MeOH formation on CZA.

ChemCatChem

Research Article
doi.org/10.1002/cctc.202500824

Chemistry Europe
European Chemical
Societies Publishing

on the overall reaction mechanism. Potentially significant differences between the reaction mechanisms on CZ and CZA occur for processes [5], [7], [8], [9], [11], [15], [24], [29], and [42] with differences of more than 0.2 eV in the reaction energy or/and the activation barrier compared to the CZ system (Supporting Information Table S10). Of these processes, only [7], [8], and [11] play a direct role for the formation of methanol via the formate mechanism, which we will discuss in more detail. The remaining processes are discussed in the Supporting Information.

3.4. Processes [8] and [7]+[12]- Hydrogenation of Formaldehyde

The formation of a methoxy unit is considered to be a key process for MeOH synthesis. Indeed, the methoxy-moiety has been reported to be present during the reaction in spectroscopic studies,[81,90,94–97] though it is important also to consider the role of MeO* as a poison, an intermediate, or both.

Methoxy formation via formaldehyde hydrogenation (process [8]) is highly exothermic for both CZ and CZA, and more so for the former ($\Delta E = -1.01$ versus -0.57 eV for CZA), and the calculations found low and modest activation barriers for CZ and CZA, respectively ($E_a(CZ) = 0.14$ eV, $E_a(CZA) = 0.41$ eV), suggesting that formaldehyde is quickly converted to methoxy. The differences between CZ and CZA can be attributed to differences in the stabilities of the initial state $H_2CO* + H*$ and the final methoxy state (Supporting Information, Tables S7 and S8). Inspection of the adsorbate geometries reveals that the only significant structural difference is the elongation of the $C=O$ bond of formaldehyde on CZA, at 1.40 versus 1.33 Å for CZA and CZ, respectively, suggesting that the $C=O$ bond is weakened as a result of the stronger formaldehyde binding on CZA (cf. next section). Still, the BCA does not suggest any significant difference in terms of partial reduction of the $C=O$ bond, which appears to be similar for both systems. As such, H_2CO* is only slightly more stabilized on CZA, compared to CZ. Process [8] has a higher activation barrier and is less exothermic on CZA, which has important implications for the overall selectivity, since the reverse process is more likely to occur at a higher rate on CZA than on CZ.

Since methoxy hydrogenation to methanol is a highly energy-demanding process, on the CZA system, reverting back to formaldehyde is likely to out-compete hydrogenation to MeO*. This in turn makes the alternative hydrogenation of formaldehyde to H_2COH* (process [7]), and then to methanol (process [12]), much more feasible. The presence of Al, then, can be interpreted to limit the impact of methoxy to acting as a spectator, or perhaps even a poison, by making the reverse of its formation competitive against the high barrier for methoxy hydrogenation to methanol (next section).

3.5. Process [11] – Formation of MeOH, Methoxy Hydrogenation

Although the calculations suggest that reversible methoxy formation via formaldehyde hydrogenation could enable methanol

formation via H_2COH*, it remains clear that when Al is present, methoxy is likely to be present in high concentrations at the active site owing to its stability (Table 3). However, the presence of Al destabilizes methoxy in our calculations (Table 3) while the activation barrier for the hydrogenation of methoxy to methanol (process [11]) is higher by 0.21 eV for the CZA versus the CZ model with the process being more endothermic by 0.12 eV. Overall, [11] is the most energy demanding process for MeOH formation via methoxy on both the CZ and CZA surfaces. The higher barrier and higher endothermicity for methoxy hydrogenation to methanol on CZA can be understood in terms of the presence of Al enhancing the stability of coadsorbed MeO* and H*, the initial state configuration for methoxy hydrogenation to methanol, and slightly destabilizing MeOH*. For both systems, the methoxy and hydrogen species are essentially competing for partial reduction; even though the BCA suggests a comparable charge accumulation on both species adsorbed on CZ and CZA (Supporting Information, Tables S7 and S8), its formation from $CO_{2(g)}$ and $H_{2(g)}$ is less exothermic on the CZ surface. The additional electron, contribute by Al, can be interpreted to alleviate the competition between the two adsorbates for electron density from the substrate, thus stabilizing coadsorbed MeO* and H* on CZA. Consequently, the higher barrier for methoxy hydrogenation to methanol means that methoxy can be considered a mechanistic "dead end" for the CZA system, with methoxy probably acting as a spectator, or a poison, rather than an intermediate. However, this makes the alternative pathway via the H_2COH intermediate a more feasible mechanism for methanol production. Examining the competing processes, we see that it is less energy-demanding for methoxy to revert to H_2CO* (with a moderate E_a of 0.98 eV [r-8] compared to 1.30 eV for methoxy hydrogenation). Hence, methoxy formation can be regarded as essentially reversible (albeit with a much lower frequency for reverting to formaldehyde), whereas hydrogenation of formaldehyde to H_2COH*, while occurring less frequently than methoxy formation, subsequently results in H_2COH* hydrogenation to methanol. Methanol can then either desorb to the gas phase, as a product, or dissociate back to H_2COH* or methoxy, but in any case, it is highly likely that H_2COH* is the only intermediate that ultimately leads to methanol formation.

3.6. Stability of Specific Species on the Interfacial Site CZA Versus CZ

It is clear that on complex catalyst surfaces, which present multiple distinct adsorption sites, the stability of a given species will vary depending on the adsorption site. Therefore, while some species may be relevant to the catalytic reaction at one site, they may not be relevant to catalysis, when adsorbed on another site. In order to rationalize the differences in binding energies of multiple intermediates at different sites on the CZ and CZA surfaces in electronic terms, calculations were performed to obtain density of states (DOS) plots and work functions for both systems (Supporting Information, Figure S1). It is clear that substituting a single bulk Zn for Al implies the presence of an additional electron, and the localization of this electron is likely to have

ChemCatChem

Research Article
doi.org/10.1002/cctc.202500824

**Chemistry
Europe**
European Chemical
Societies Publishing

Table 3. Relative stabilities and BCA electron excess (*in italic*) of a variety of key carbon-species on a surface site (A, B, or D) as presented in our publication.[58] All values are referenced to the gaseous species noted in the last row. The most stable or/and activated species are highlighted in bold.

Site / Species	HCOO*) CZ	CZA	CO₂*) CZ	CZA	CO*) CZ	CZA	H₂CO*) CZ	CZA	H₃CO*) CZ	CZA
	$HCOO^{*)}$		$CO_2^{*)}$		$CO^{*)}$		$H_2CO^{*)}$		$H_3CO^{*)}$	
	CZ	CZA	CZ	CZA	CZ	CZA	CZ	CZA	CZ	CZA
Cu/Zn (A)	−1.28	−1.13	−0.41	−0.42	−0.72	−1.12**)	**−1.02**	**−1.20**	−1.76	−1.55
BCA e^- excess	*0.59*	***0.64***	***0.77***	***0.88***	***0.36***	*0.10*	***0.84***	***0.91***	*0.57*	*0.56*
Zn (D)	−1.40	−1.49	**−0.86**	**−0.87**	−0.64	−0.67	−0.88	−0.95	−1.02	−1.13
BCA e^- excess	***0.63***	*0.58*	*0.35*	*0.39*	*−0.09*	*−0.14*	*0.04*	*0.17*	***0.72***	***0.79***
Cu (B)	**−1.95**	**−2.41**	−0.37	−0.51	**−1.28**	**−1.31**	−0.50	−0.69*)	−1.20	−1.06
BCA e^- excess	*0.57*	*0.63*	*0.65*	*0.33*	*0.29*	***0.31***	*0.27*	*0.54*	*0.52*	*0.52*
Reference	$CO_{2(g)}$ + 3 $H_{2(g)}$		$CO_{2(g)}$		$CO_{(g)}$		$H_2CO_{(g)}$		$CO_{2(g)}$ + 3 $H_{2(g)}$	

* This geometry is rotated and more stable as the one reported in CZ. The structure on CZ has the same stability on both systems (*cf.* Supporting Information);

** This site resembles a Cu site, but it is close to the A site, and this is the only structure that was found.

implications for adsorption and catalytic processes. Although the present model cannot accommodate phenomena such as crystallite grain boundary defects, and the possibility of electron localization at such sites, the charge density difference plots (Figure S1) suggest electron localization takes place at the Cu/ZnO interface, and is enhanced for the CZA system at the interfacial A site which we focus on as the main catalytic site for CO_2 activation and subsequent methanol formation in our model system. Furthermore, the DOS and work function calculations show that, relative to a common vacuum level, the Fermi level for our CZA model lies above that of CZ by 0.17 eV, implying population of conduction band-like levels. In terms of the implications for adsorption, this result suggests that electron donation from CZA to higher lying molecular orbital levels may facilitate binding on CZA, compared to CZ. However, it does not necessarily mean that all intermediates would be more activated or show greater stability on the CZA versus the CZ model, given the differences in charge localization at different surface sites, as illustrated by the charge density difference plots in Figure 1 (II). In Table 3, the relative binding energies for a variety of key species are presented, to illustrate the impact of the single bulk Al atom on the adsorption and binding of a variety of key species. The stability of formate and its repercussions will be discussed in the next section.

The calculations show that CO* binds most strongly on Cu sites (A and B sites), with the BCA showing partial CO reduction in both cases with especially strong binding at the Cu-only B site, in agreement with the well reported observation of Cu carbonyls.[99] However, the calculations also show strong binding of CO on the Zn site, although the BCA suggests that no partial reduction of CO occurs in this case (BCA, Table 3, *cf.* general for nonclassical carbonyls[99]) At the A site electron donation can stabilize CO, with the presence of both Zn and Cu facilitating limited partial reduction. In contrast, on the Zn (D) site, only weak oxidation of CO is observed from the Bader charge analysis, perhaps originating from interaction with surface O rather than Zn. Notably, any attempt to adsorb CO at the interfacial Cu/Zn A site on CZA resulted in the optimized adsorption structure migrating to an adjacent Cu-only site (similar to the Cu-only

B site), which is in agreement with the experiment that shows that gaseous CO introduced via the input gas feed is not the reactive species for methanol formation,[47,100–102] since it cannot bind to the interfacial A site in CZA. Rather, the calculations suggest that CO can only be accommodated at the interfacial Cu/Zn A site, when coadsorbed with O*, which means via CO_2 dissociation as reported in process [3], as can be understood in terms of the coadsorbed O*$_B$ species enhancing the Lewis acidity of the surface, thus making the interfacial A site active for CO binding.

Overall, formaldehyde is calculated to bind more strongly on all sites on CZA compared to CZ and for example, adsorption is more stable by at least ∼−0.10 eV on CZA. This enhanced adsorption correlates with the activation of H_2CO (Table 3), on sites with higher localization of electron density (cf. Figure 1 (II)), facilitating stronger binding and a greater extent of partial reduction of the C═O bond.

MeO$_A$* shows the same extent of charge transfer and is the most stable species at the interfacial (A) site in CZ and CZA (more stable by −0.21 eV on CZ than on CZA), but more weakly bound at the Cu (B) and Zn (D) sites. For CZ, MeO* is more strongly bound on Cu (B), whereas for CZA, MeO* is more stable at the Zn (D) site, although in all cases the adsorption energies and charge distributions are comparable. The difference could be attributed to the role of Al in providing an additional electron that makes electron transfer from the substrate to the MeO* species less energy demanding.

An analysis of the stability of H* on different sites of the CZA is commented in the Supporting Information. Although there are changes in the adsorption of H* on the interfacial sites being less exothermic on CZA compared with CZ and more exothermic on the Cu and Zn sites respectively, none of the changes are especially significant and the results are consistent with the assumption that H* is abundant on the surface.

3.7. Formate: Intermediate and Spectator

Formate has been suggested as a key intermediate for CO_2 conversion to methanol.[58,75,93,103–105] It is highly stable at the Cu/ZnO

Table 4. Comparison between different formate structures on CZA and CZ. ΔE refers to the formation of a HCOO* on each site of each system in accordance with energy of the clean surface (CZ or CZA) + $CO_{2(g)}$ + $\frac{1}{2}$ $H_{2(g)}$. No major difference in BCA difference between each formate was found, with an activation of ca. 0.6 e⁻ for each species. Sites are comparable to those shown in Figure 1. Bond lengths and other structural parameters are provided at the Supporting Information (Table S6).
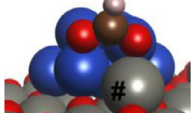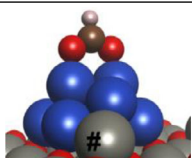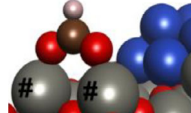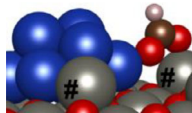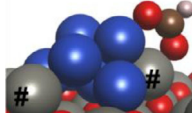
Site	Interface (A)	Top of Cu (B)	Far Zn (D)	Side (C + D)	Cu/Zn (C)
ΔE_{CZ}/ eV	−1.278	−1.951	−1.396	−1.442	−1.609
ΔE_{CZA}/ eV	−1.132	−2.414	−1.488	−1.464	−1.557

Table 5. Stabilities of O*, OH*, and H_2O* on different sites and on both CZ and CZA systems with respect to their reaction to $CO_{2(g)}$ + 3 $H_{2(g)}$ (=0 eV) for overall comparison with all other reported processes. For abbreviation, only the adsorbed species are listed, i.e., that the accompanying species from the reaction are omitted, e.g., for O* it would be O* + $H_{2(g)}$ + $MeOH_{(g)}$. Only for the water molecule, the reference is its gas phase molecule, i.e., the reported value corresponds to its adsorption energy. The most stable or/and activated species per system are highlighted in bold.

Site / Species	O*		OH*		H_2O*	
	CZ	CZA	CZ	CZA	CZ	CZA
Cu/Zn (A)	−0.73	**−1.32**	**−1.75**	**−1.57**	–	–
BCA e⁻ excess	0.87	0.89	*0.58*	*0.58*	–	–
Zn (D)	**−0.91**	−1.07	−0.29	−0.33	–	–
BCA e⁻ excess	*0.91*	*0.91*	0.55	0.56	–	–
Cu (B)	−0.44	−0.34	−1.29	−1.15	**−0.38**	**−0.36**
BCA e⁻ excess	0.70	0.70	0.51	0.50	0.09	0.09
Reference	$CO_{2(g)}$ + 3 $H_{2(g)}$				$H_2O_{(g)}$	

interfacial site A and also potentially acts as an intermediate rather than merely a spectator species, which the calculations suggest is the case for other formate adsorption configurations. Hence, here, the impact of the presence of Al on formate binding is discussed. On CZA, the stability of formate is calculated to increase significantly on the Cu site (B), and to a lesser degree on other sites. Yet, formate is slightly destabilized on the interfacial A and C sites. This finding supports the hypothesis that the prominent formate signatures observed spectroscopically correspond to high concentrations of formate spectator species bound on the Cu sites,[58] with the HCOO*$_B$ species as a predominant being more stable than the interfacial HCOO*$_A$ relevant for the mechanism (by more than 0.7 eV on CZ or 1.2 eV on CZA, Table 4).

In comparison, formate binding at the interfacial A site is modestly weakened when Al is present, with HCOO*$_A$ binding more exothermically by 0.15 eV on CZ compared to CZA. No significant changes were observed between the CZ and CZA model systems in terms of the BCA, suggesting that a similar extent of charge transfer from the surface to the adsorbate is required to stabilize formate, but the energetics of this charge transfer process differs on CZ compared to CZA, depending on the specific binding site.

3.8. The Role of Water Related Species O*/OH*/H_2O*

It is important to understand the nature of water and related species on the surface of the CZ and CZA systems. Notably, the adsorption of atomic O* at interfacial sites is enhanced for the CZA system, with the interfacial O* being more stable than O* at Cu sites by almost 1 eV. Moreover, the O* species is more exothermically bound at the interfacial A site on CZA by ca. 0.6 eV compared to the same site on the CZ system. By contrast, the most stable binding site for O* on the CZ surface is at the Zn site (Table 5), which can be interpreted in electronic terms by considering the high electronegativity of O, and the most reducing sites available on the two surfaces. For the CZ surface, the most reducing sites correspond to the undercoordinated surface Zn species,[35,106] which can undergo more complex oxidation to stabilize surface O*, essentially resembling bulk ZnO. However, for the CZA surface, the additional electron provided by Al, which becomes localized at the Cu/ZnO interface (Figure 1 (II)) facilitates stronger O binding. Hence for the CZA surface, the interfacial site A yields the most exothermic binding energy for O*, indicating the urgent need for an O*$_A$ scavenger in the mechanism.

Scavenging could potentially be achieved by adsorption of H* and formation of OH*. Here, the calculations indicate that
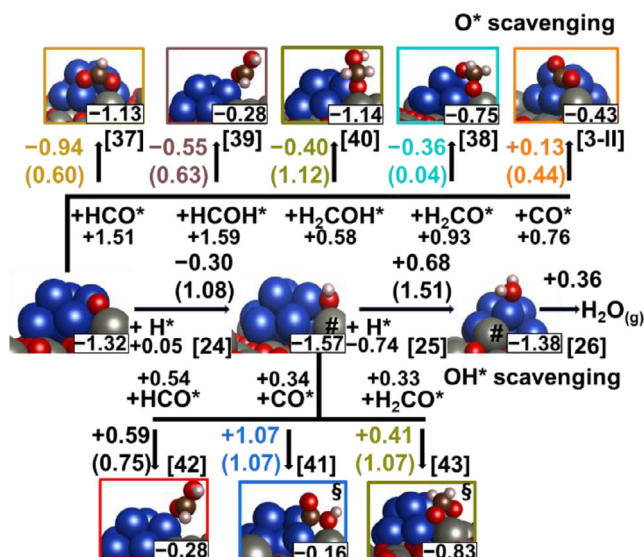
ChemCatChem

Research Article
doi.org/10.1002/cctc.202500824

Chemistry
Europe
European Chemical
Societies Publishing

Figure 4. Scheme of possible reaction pathways for O/OH* scavenging of the interfacial site A of CZA as shown in our publication.[58] Stabilities of the species are given with respect to their reaction to $CO_{2(g)} + 3\,H_{2(g)}$ (=0 eV). Only processes involving O/OH* on the A site are shown; all processes are listed in Table 2. E_a's are listed in parentheses in eV (X), process numbers in brackets [Y] and elementary processes are given above the E_a's. Only transition states and starting structures that change from CZ to CZA are included in the Supporting Information of this manuscript.

OH* is also one of the most stable species on the A site, although 0.18 eV more stable on CZ than on CZA. A similar trend is observed on the Cu site, suggesting that on the CZA, Cu plays a more significant role in the stabilization of OH* rather than the Zn component. Yet, the formation of OH*$_A$ from hydrogenation of O*$_A$ is less exothermic and has a higher activation barrier for CZA compared to CZ ([24], on CZA: $E_a = 1.08$ eV, $\Delta E = -0.30$ eV versus on CZ: $E_a = 0.79$ eV, $\Delta E = -0.66$ eV).

Hence, given that there are other O*$_A$ scavenging path options (Figure 4), the presence of Al could possibly limit poisoning of active interfacial sites by OH*, since OH* is less stable on CZA and its formation is less exothermic and more energy demanding. The BCA shows no big changes in the electron density donation and similar destabilization is seen for HCOO* and MeO* on CZA versus on CZ. Further hydrogenation of OH* to water on the A site is challenging on the CZA surface, as is the case for the CZ system.[58] Although the hydrogenation of OH*$_A$ is less endothermic (0.68 eV) on CZA, this process [25] has a higher activation barrier ($E_a = 1.51$ eV) compared to that reported for the CZ system ($\Delta E = 0.89$ eV, $E_a = 1.34$ eV), and as such, the process is unlikely to play a major role in the formation of water on the A site. In contrast, the same process on Cu sites (process [25B]) has a much lower activation barrier and thus is likely to be more feasible for CZA ($\Delta E = 0.23$ eV, $E_a = 0.84$ eV) compared to CZ ($\Delta E = 0.23$ eV, $E_a = 0.91$ eV), suggesting slow water formation on Cu sites. For the coadsorption configuration OH* + H*, the initial state for water formation, the results show that this coadsorption configuration is more stable on CZ compared to CZA (Table 6).

The differences in the calculated adsorption and activation of adsorbed water on the same interfacial site on CZ and CZA

are not significant for Cu sites (B-I and -II). However, the H2O molecule bound at site C is much more stable on the CZA than on the CZ model. As expected, and reported in our previous work,[58] the adsorption of water on the Cu/ZnO systems is problematic, which is corroborated by our calculations. Water formation appears particularly feasible on a site with a stronger Zn site character (C), and to a lesser extent on Cu sites. The relationship between adsorbate stability, and the extent of partial reduction as evaluated from the BCA, is to be reversed for H_2O^* compared to CO_2^*: while chemisorbed CO_2^* is found to be highly stable, regardless of the extent of partial reduction, H_2O^* adsorbed at the C site is less stable, despite a great extent of partial reduction, as is evident from the BCA. In agreement, CO_2^* can easily accommodate additional electron density by partial reduction of the $C{=}O$ π^* orbitals. For H_2O, the lack of suitable empty orbitals at low energy implies that the partial reduction leads to a significant destabilization of the H_2O^* molecule (cf. OH*A stability)
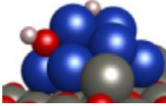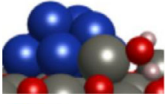
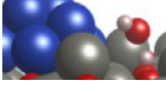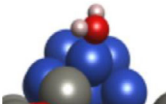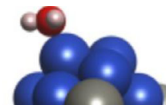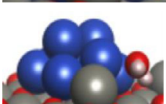### 3.9. O/OH* Scavenging on Cu and Cu/ZnO Surfaces

With O* being moderately stable at the interfacial A site, there must be other paths to restore the active site. The calculations suggest that all the processes considered appear to be feasible (some with low activation barriers, e.g., [38], others with moderate activation barriers, [37], [39], [3-II], and some with much higher activation barriers [40], Figure 4). These processes are energetically favored by, e.g., the formation of highly stable intermediates such as HCOO*, H_2COOH^*, H_2COO^*, or by the formation of species that would be rapidly consumed immediately after formation like CO_2^* or HCOOH*, thus favoring O* scavenging. CO_2^*, for example, would readily convert to formate (process [37]). Similarly, any HCOOH* formed is likely to dissociate to HCOO* and H* ([r15]), undergo hydrogenation to H_2COOH^* ([22]), or dissociate to OH*$_A$ and HCO*$_B$ ([r42]) (Supporting Information, Figure S4).

Hence, there are plenty of feasible processes to restore the active interfacial site A for the methanol formation mechanism.

4. Summary and Conclusions

Our calculations provide further insights into the role of Al in our model CZA catalyst, and thus by extension, the industrial $Cu/ZnO/Al_2O_3$ catalyst used for methanol production. Although alumina is often considered as a structural promoter, the present work demonstrates how dilute Al can also act as an effective electronic dopant of the catalyst, with the relative stabilities of various key species being correlated with electronic interactions that can ultimately enhance reactivity toward methanol formation compared to the undoped CZ system.[58] The repercussions vary between de/stabilization of key start- or, end states and intermediates (formate, methoxy, CO*, CO_2^*, and formaldehyde), different transition states, e.g., slowing down processes of MeO* hydrogenation to methanol favoring HCO* hydrogenation to HCOH* or hydrogenation of H_2COO^* to H_2COOH^*. Adsorption

ChemCatChem

Research Article
doi.org/10.1002/cctc.202500824

Chemistry Europe
European Chemical
Societies Publishing

Table 6. Energy of adsorption/formation and activation of species related to $H_2O(g)$ on CZ and CZA. Structures are closely related to the ones reported for CZ.

Species OH* + H*	Structure	CZA ΔE/ eV	$\beta_{OH/H}$	CZ ΔE/eV	$\beta_{OH/H}$
OH*$_B$ + H*$_{B-I}$		−1.50	0.49/0.50	−1.57	0.51/0.86
OH*+ H* A		−1.77	0.51/−0.20	−1.90	0.60/0.11
OH*+ H* D		**−1.95**	0.47/−0.04	**−2.11**	0.38/−0.06
H$_2$O* / Site		ΔE/ eV	β_{H2O}	ΔE/ eV	β_{H2O}
H$_2$O B-I		−0.36	0.09	−0.38	0.07
H$_2$O B-II		−0.57	−0.03	**−0.64**	0.14
H$_2$O C		**−0.99**	0.26	−0.50	0.34

geometries, as well as electronic bands of the doped system are changed affecting the overall reaction to methanol formation. Our analysis of every step toward methanol formation, emphasizes the electronic role of aluminium in comparison to the undoped Cu/ZnO system previously reported.

We have found that the presence of Al can potentially induce a deviation from the "classical" formate path for methanol formation on the CZA model surface: The high stability of the methoxy unit at the interfacial site A and the difficulty of its hydrogenation to methanol makes MeO*$_A$ irrelevant for the mechanism. Conversely, the hydroxymethyl intermediate, H$_2$COH*$_A$, now plays the relevant role for methanol-formation, avoiding the energy demanding methoxy hydrogenation. We note that the calculations suggest that processes consuming the H$_2$COH*$_A$ species have low activation barriers and are likely to occur rapidly, thus probably precluding its observation in surface spectroscopic studies. Conversely, the highly stable and readily observed MeO*$_A$-moiety represents a mechanistic dead-end for methanol synthesis, acting as a spectator or even poison, rather than an intermediate. The results also demonstrate the impact of the presence of Al on formate species, with the active interfacial Cu/ZnO formate being destabilized, and thus more active, while formate species located on other surface adsorption site are stabilized to a greater extent. It is therefore proposed that these nonactive spectator formate species correspond to those reported from surface spectroscopy. Indeed, if methoxy hydrogenation is avoided, the most energy-demanding process

calculated is instead the hydrogenation of formate to form dioxomethylene (process [16], $E_a = \sim 1.10$ eV) on the doped CZA system. This change apparently makes the overall methanol formation process faster and more selective on CZA than on CZ.

Furthermore, the RWGS-path including CO_2 dissociation, and subsequent CO hydrogenation, could also contribute to overall methanol formation, albeit as a minority pathway, with this mechanism competing against the formate path. CO adsorbs on the active site only with the help of O* increasing its Lewis acidic character and can further react to HCO* until the formaldehyde state is reached. That the RWGS path was found to potentially contribute to methanol formation on CZA, and in contrast to the CZ system, demonstrates the impact of a low levels of aluminium dopants (in our model a single atom in the bulk out of a total of ~260 atoms in the slab model) on possible surface reaction pathways. As such, the results obtained in the present work provide motivation for further experimental investigations to understand better the role of dilute Al in the industrial CZA catalyst.

Changes in stability are also reported for water and its related species upon the introduction of Al. Although the formation of water is expected on the Cu site of the CZA surface, as is the case for CZ, for the CZA model system Zn sites also exhibit enhanced water adsorption. The results suggest that the Cu/ZnO interfacial site plays a lesser role in the formation of water, thus avoiding potential competition between methanol and water formation. The Cu/ZnO interfacial site shows nevertheless high stability for

ChemCatChem

Research Article
doi.org/10.1002/cctc.202500824

**Chemistry
Europe**
European Chemical
Societies Publishing

O* and OH* species. Though formation of the latter is energetically demanding on the CZA interfacial site, its stability is high overall on Cu. Yet, for the CZA model, OH* does not represent a poison to the catalyst methanol active site, as our results also show that O* scavenging processes are available, leaving OH* formation step less feasible. However, it must be acknowledged that while the results represent a complete electronic analysis of the effects of Al on the system, the model applied in the present work represents a minimal model intended to investigate the impact of the presence of dilute Al in contrast with the results obtained for the benchmark CZ system, and thus does not include the structural effects of the dopant Al atom. In a real catalyst system, isolated Al atoms are likely to be present at a variety of different sites, including those at the surface, that may have a high affinity for water, and therefore potentially "drown" the catalyst surface. Further investigation into this phenomenon is required, but lies outside the scope of the present work.

In conclusion, the present work demonstrates the electronic role of Al in affecting the surface reaction processes relevant to the formation of methanol on a model CZA catalyst surface by enhancing the concentration of conduction band electrons such that key intermediates, such as methoxy and formate, and their H-coadsorbed counterparts, are stabilized or destabilized in a way that favors a less energy-demanding mechanistic pathway to achieve methanol formation. Our results show that aluminium can influence selectivity toward methanol, and potentially even provide an alternative to the established mechanism of formation avoiding the MeO*-unit, now assigned as spectator, and allowing a contribution of the RWGS path, and increases the activity due to lowering the overall reaction barriers. Even the presence of dilute Al localized within the ZnO bulk site creates a plate ensemble of opportunities to tune the catalyst of MeOH formation, showing in the interfacial site the active site for MeOH formation. This work represents a guide to understanding the Al doping character on the electronic contributions, enabling scientists to further understand complex mechanisms, which will be explored in more detail in future work using kinetic Monte Carlo techniques.

Supporting Information

The supporting information is available free of charge and contains: Further Methodology: Parameters for DOS calculations, parameters for calculations of activation barriers via CI-NEB and IDM, Justification of the Model: DOS plots for CZ and CZA, data without ZPE correction. Further analysis of different paths of MeOH formation: Hydrogen adsorption and dissociation, additional graphics for remaining elementary steps and their transition states, additional vibrational values for comparison to the experiment.

Author Contributions

All authors conceived and designed the research program. The studies and investigations were conducted by D.A.J.A. with the support of all authors. The initial version of the manuscript was written by D.A.J.A and M.D.H., edited, revised, and improved by C.R.A.C. and I.K., and approved by all authors.

Conflict of Interests

The authors declare no conflict of interest.

Data Availability Statement

All data supporting this work is available in the manuscript and Supporting Information.

[1] J. Ott, V. Gronemann, F. Pontzen, E. Fiedler, G. Grossmann, D. B. Kersebohm, G. Weiss, C. Witte, in *Ullmann's Encyclopedia of Industrial Chemistry*, Wiley-VCH Verlag GmbH & Co. KGaA, Weinheim, Germany, **2012**.

[2] R. Malhotra, *Fossil Energy. Selected Entries from the Encyclopedia of Sustainability Science and Technology*, Springer, New York, **2013**.

[3] J. T. Gallagher, J. M. Kidd, GB1159035A **1969**.

[4] *Handbook of heterogeneous catalysis*, Ed: (G. Ertl), Wiley-VCH, Weinheim, Chichester, **2008**.

[5] B. Collins, US3850850A, **1974**.

[6] M. R. Gogate, *Pet. Sci. Technol.* **2019**, *37*, 603–610.

[7] G. Pacchioni, *ACS Catal.* **2024**, *14*, 2730–2745.

[8] A. E. A. Gent, US3950369A, **1976**.

[9] P. Friedlingstein, J. Matthew, W. M. O'Sullivan, R. Andrew, D. Bakker, J. Hauck, C. Le Quéré, G. Peters, W. Peters, J. Pongratz, et al., *Supplemental data of Global Carbon Budget* 2023, *2023*, Global Carbon Project.

[10] C. Le Quéré, R. B. Jackson, M. W. Jones, A. J. P. Smith, S. Abernethy, R. M. Andrew, A. J. De-Gol, D. R. Willis, Y. Shan, J. G. Canadell, et al., *Nat. Clim. Change* 2020, *10*, 647.

[11] X. Lim, *Nature News* 2015, *526*, 628-630.

[12] GlobalData, "Production capacity of methanol worldwide from 2018 to 2022 | Statista" can be found under https://www.statista.com/statistics/1065891/global-methanol-production-capacity/, last access 18.02.2025, 2023.

[13] T. Hisatomi, Q. Wang, F. Zhang, S. Ardo, E. Reisner, H. Nishiyama, A. Kudo, T. Yamada, K. Domen, *Front. Sci.* 2024, *2*, 1–21.

[14] T. Hisatomi, K. Domen, *Faraday Discuss.* 2017, *198*, 11-35.

[15] G. Segev, J. Kibsgaard, C. Hahn, Z. J. Xu, W.-H. (S.) Cheng, T. G. Deutsch, C. Xiang, J. Z. Zhang, L. Hammarström, D. G. Nocera, A. Z. Weber, P. Agbo, T. Hisatomi, F. E. Osterloh, K. Domen, F. F. Abdi, S. Haussener, D. J. Miller, S. Ardo, P. C. Mcintyre, T. Hannappel, S. Hu, H. Atwater, J. M. Gregoire, M. Z. Ertem, I. D. Sharp, K.-S. Choi, J. S. Lee, O. Ishitani, et al., *J. Phys. D: Appl. Phys.* 2022, *55*, 323003.

[16] J. Jia, L. C. Seitz, J. D. Benck, Y. Huo, Y. Chen, J. W. D. Ng, T. Bilir, J. S. Harris, T. F. Jaramillo, *Nat. Commun.* 2016, *7*, 13237.

[17] K. Maeda, K. Domen, *J. Phys. Chem. Lett.* 2010, *1*, 2655–2661.

[18] M. R. Shaner, H. A. Atwater, N. S. Lewis, E. W. McFarland, *Energy Environ. Sci.* 2016, *9*, 2354–2371.

[19] J. S. Lee, *Catal. Surv. Asia* 2005, *9*, 217–227.

[20] K. Maeda, K. Domen, *J. Phys. Chem. C* 2007, *111*, 7851–7861.

[21] F. E. Osterloh, *Chem. Mater.* 2008, *20*, 35–54.

[22] A. Kudo, Y. Miseki, *Chem. Soc. Rev.* 2009, *38*, 253-278.

[23] W. J. Youngblood, S.-H. A. Lee, K. Maeda, T. E. Mallouk, *Acc. Chem. Res.* 2009, *42*, 1966–1973.

[24] H. Bai, A. C. Yeh, *Ind. Eng. Chem. Res.* 1997, *36*, 2490–2493.

[25] K. Nakagawa, T. Ohashi, *J. Electrochem. Soc.* 1998, *145*, 1344–1346.

[26] Q. Li, Q. S. Yu, J. Jiang, Z. X. Zhang, *Journal of Chemical Engineering of Chinese Universities* 2010, *24*, 29–34.

[27] G. A. Olah, A. Goeppert, G. K. S. Prakash, *Beyond Oil and Gas: The Methanol Economy*, Wiley-VCH, Weinheim, 2018.

[28] G. C. Chinchen, P. J. Denny, D. G. Parker, M. S. Spencer, D. A. Whan, *Appl. Catal.* 1987, *30*, 333–338.

[29] V. D. Dasireddy, B. Likozar, *Renewable Energy* 2019, *140*, 452–460.

[30] J. Skrzypek, M. Lachowska, M. Grzesik, J. Słoczyński, P. Nowak, *Chem. Eng. J.* 1995, *58*, 101.

[31] K. Klier, *J. Catal.* 1982, *74*, 343–360.

[32] M. Kurtz, H. Wilmer, T. Genger, O. Hinrichsen, M. Muhler, *Catal. Lett.* 2003, *86*, 77–80.

[33] S. J. Tauster, *Acc. Chem. Res.* 1987, *20*, 389–394.

[34] M. Behrens, *J. Catal.* 2009, *267*, 24–29.

[35] M. Behrens, F. Studt, I. Kasatkin, S. Kühl, M. Hävecker, F. Abild-Pedersen, S. Zander, F. Girgsdies, P. Kurr, B.-L. Kniep, M. Tovar, R. W. Fischer, J. K. Nørskov, R. Schlögl, *Science* 2012, *336*, 893–897.

[36] T. Lunkenbein, J. Schumann, M. Behrens, R. Schlögl, M. G. Willinger, *Angew. Chem.* 2015, *127*, 4627-4631.

[37] J. Nakamura, *Top. Catal.* 2003, *22*, 277–285.

[38] M. S. Spencer, *Surf. Sci.* 1987, *192*, 323–328.

[39] M. S. Spencer, *Surf. Sci.* 1987, *192*, 329–335.

[40] M. S. Spencer, *Surf. Sci.* 1987, *192*, 336–343.

[41] T. Fujitani, I. Nakamura, T. Uchijima, J. Nakamura, *Surf. Sci.* 1997, *383*, 285–298.

[42] D. Kordus, J. Jelic, M. Lopez Luna, N. J. Divins, J. Timoshenko, S. W. Chee, C. Rettenmaier, J. Kröhnert, S. Kühl, A. Trunschke, R. Schlögl, F. Studt, B. Roldan Cuenya, *J. Am. Chem. Soc.* 2023, *145*, 3016–3030.

[43] T. Vanherwijnen, *J. Catal.* 1974, *34*, 209–214.

[44] G. J. Millar, C. H. Rochester, C. Howe, K. C. Waugh, *Mol. Phys.* 1992, *76*, 833–849.

[45] B. Xie, R. J. Wong, T. H. Tan, M. Higham, E. K. Gibson, D. Decarolis, J. Callison, K.-F. Aguey-Zinsou, M. Bowker, C. R. A. Catlow, J. Scott, R. Amal, *Nat. Commun.* 2020, *11*, 1615.

[46] J. Graciani, K. Mudiyanselage, F. Xu, A. E. Baber, J. Evans, S. D. Senanayake, D. J. Stacchiola, P. Liu, J. Hrbek, J. F. Sanz, J. A. Rodriguez, *Science* 2014, *345*, 546–550.

[47] F. Studt, M. Behrens, E. L. Kunkes, N. Thomas, S. Zander, A. Tarasov, J. Schumann, E. Frei, J. B. Varley, F. Abild-Pedersen, et al., *Chem. Cat. Chem.* 2015, *7*, 1105.

[48] M. Heenemann, M.-M. Millet, F. Girgsdies, M. Eichelbaum, T. Risse, R. Schlögl, T. Jones, E. Frei, *ACS Catal.* 2020, *10*, 5672–5680.

[49] T. Reichenbach, K. Mondal, M. Jäger, T. Vent-Schmidt, D. Himmel, V. Dybbert, A. Bruix, I. Krossing, M. Walter, M. Moseler, *J. Catal.* 2018, *360*, 168–174.

[50] J. Hu, Y. Song, J. Huang, Y. Li, M. Chen, H. Wan, *Chem. - Eur. J.* 2017, *23*, 10632–10637.

[51] M. Behrens, S. Zander, P. Kurr, N. Jacobsen, J. Senker, G. Koch, T. Ressler, R. W. Fischer, R. Schlögl, *J. Am. Chem. Soc.* 2013, *135*, 6061–6068.

[52] M. Behrens, G. Lolli, N. Muratova, I. Kasatkin, M. Hävecker, R. N. d'Alnoncourt, O. Storcheva, K. Köhler, M. Muhler, R. Schlögl, *Phys. Chem. Chem. Phys.* 2013, *15*, 1374–1381.

[53] N. Narkhede, H. Zheng, H. Zhang, G. Zhang, Z. L. Li, *Catal. Sci. Technol.* 2020, *10*, 7386–7398.

[54] Y.-H. Zhang, Y.-L. Li, F.-L. Gong, K.-F. Xie, M. Liu, H.-L. Zhang, S.-M. Fang, *Sens. Actuators, B, Chem.* 2020, *305*, 127489.

[55] D. Mora-Fonz, T. Lazauskas, M. R. Farrow, C. R. A. Catlow, S. M. Woodley, A. A. Sokol, *Chem. Mater.* 2017, *29*, 5306–5320.

[56] D. Mora-Fonz, T. Lazauskas, S. M. Woodley, S. T. Bromley, C. R. A. Catlow, A. A. Sokol, *J. Phys. Chem. C* 2017, *121*, 16831–16844.

[57] M. D. Higham, D. Mora-Fonz, A. A. Sokol, S. M. Woodley, C. R. A. Catlow, *J. Mater. Chem. A* 2020, *8*, 22840–22857.

[58] D. Jurado A, M. D. Higham, Y. R. Poh, C. R. A. Catlow, I. Krossing, *J. Catal.* 2025, *446*, 115997.

[59] G. Kresse, J. Furthmüller, *Comput. Mater. Sci.* 1996, *6*, 15–50.

[60] G. Kresse, J. Furthmüller, *Phys. Rev. B* 1996, *54*, 11169–11186.

[61] G. Kresse, J. Hafner, *Phys. Rev. B* 1993, *47*, 558–561.

[62] G. Kresse, J. Hafner, *Phys. Rev. B* 1994, *49*, 14251–14269.

[63] P. E. Blöchl, *Phys. Rev. B* 1994, *50*, 17953.

[64] J. P. Perdew, A. Ruzsinszky, G. I. Csonka, O. A. Vydrov, G. E. Scuseria, L. A. Constantin, X. Zhou, K. Burke, *Phys. Rev. Lett.* 2008, *100*, 136406.

[65] G. Kresse, D. Joubert, *Phys. Rev. B* 1999, *59*, 1758–1775.

[66] X. Qu, W. Wang, S. Lv, D. Jia, *Solid State Commun.* 2011, *151*, 332–336.

[67] S. A. French, A. A. Sokol, C. R. A. Catlow, P. Sherwood, *J. Phys. Chem. C* 2008, *112*, 7420–7430.

[68] S. A. French, A. A. Sokol, S. T. Bromley, C. R. A. Catlow, P. Sherwood, *Top. Catal.* 2003, *24*, 161–172.

[69] M. D. Higham, M. G. Quesne, C. R. A. Catlow, *Dalton Trans.* 2020, *49*, 8478–8497.

[70] C. R. A. Catlow, S. A. French, A. A. Sokol, M. Alfredsson, S. T. Bromley, *Faraday Discuss.* 2003, *124*, 185.

[71] B. J. Da, S. Bronsato, E. F. Souza, G. G. Gonzalez, L. H. Chagas, P. C. Zonetti, C. D. Mendoza, N. Raquel Checca Huaman, R. R. de Avillez, L. G. Appel, *Fuel* 2024, *375*, 132533.

[72] N. Narkhede, H. Zheng, H. Zhang, G. Zhang, Z. Li, *Chem. Cat. Chem.* 2020, *12*, 5697.

[73] K. Momma, F. Izumi, *J. Appl. Crystallogr.* 2011, *44*, 1272-1276.

[74] T. Pinheiro Araújo, G. Giannakakis, J. Morales-Vidal, M. Agrachev, Z. Ruiz-Bernal, P. Preikschas, T. Zou, F. Krumeich, P. O. Willi, W. J. Stark, R. N. Grass, G. Jeschke, S. Mitchell, N. López, J. Pérez-Ramírez, *Nat. Commun.* 2024, *15*, 3101.

[75] S. Kattel, P. J. Ramírez, J. G. Chen, J. A. Rodriguez, P. Liu, *Science* 2017, *355*, 1296–1299.

[76] S. M. Gericke, M. M. Kauppinen, M. Wagner, M. Riva, G. Franceschi, A. Posada-Borbón, L. Rämisch, S. Pfaff, E. Rheinfrank, A. M. Imre, et al., *ACS Appl. Mater. Interfaces* 2023, *15*, 45367–45377.

[77] X. Wang, H. Zhang, H. Qin, K. Wu, K. Wang, J. Ma, W. Fan, *Fuel* 2023, *346*, 128381.

[78] K. Wang, D. Liu, L. Liu, J. Liu, X. Hu, P. Li, M. Li, A. S. Vasenko, C. Xiao, S. Ding, *eScience* 2022, *2*, 518–528.

[79] X. Huang, A. Beck, A. Fedorov, H. Frey, B. Zhang, B. Klötzer, J. A. van Bokhoven, C. Copéret, M.-G. Willinger, *Chem. Cat. Chem.* 2022, *14*, e202201280.

[80] E. Lam, J. J. Corral-Pérez, K. Larmier, G. Noh, P. Wolf, A. Comas-Vives, A. Urakawa, C. Copéret, *Angew. Chem., Int. Ed.* 2019, *58*, 13989–13996.

[81] L. C. Grabow, M. Mavrikakis, *ACS Catal.* **2011**, *1*, 365–384.

[82] G. Dutta, A. A. Sokol, C. R. A. Catlow, T. W. Keal, P. Sherwood, *ChemPhysChem* **2012**, *13*, 3453–3456.

[83] N. J. Divins, D. Kordus, J. Timoshenko, I. Sinev, I. Zegkinoglou, A. Bergmann, S. W. Chee, S. Widrinna, O. Karslıoğlu, H. Mistry, M. Lopez Luna, J. Q. Zhong, A. S. Hoffman, A. Boubnov, J. A. Boscoboinik, M. Heggen, R. E. Dunin-Borkowski, S. R. Bare, B. R. Cuenya, *Nat. Commun.* **2021**, *12*, 1435.

[84] C. Tisseraud, C. Comminges, S. Pronier, Y. Pouilloux, A. Le Valant, *J. Catal.* **2016**, *343*, 106–114.

[85] O. Martin, C. Mondelli, D. Curulla-Ferré, C. Drouilly, R. Hauert, J. Pérez-Ramírez, *ACS Catal.* **2015**, *5*, 5607–5616.

[86] E. A. Volnina, M. A. Kipnis, *Kinet. Catal.* **2020**, *61*, 119–129.

[87] Y. Yang, J. Evans, J. A. Rodriguez, M. G. White, P. Liu, *Phys. Chem. Chem. Phys.* **2010**, *12*, 9909.

[88] J. Yoshihara, S. C. Parker, A. Schafer, C. T. Campbell, *Catal. Lett.* **1995**, *31*, 313–324.

[89] G. C. Chinchen, K. C. Waugh, D. A. Whan, *Appl. Catal.* **1986**, *25*, 101–107.

[90] S. M. Fehr, K. Nguyen, I. Krossing, *Chem. Cat. Chem.* **2022**, *14*, e202101500.

[91] S. M. Fehr, I. Krossing, *Chem. Cat. Chem.* **2020**, *12*, 2622.

[92] M. Nadjafi, A. M. Kierzkowska, A. Armutlulu, R. Verel, A. Fedorov, P. M. Abdala, C. R. Müller, *J. Phys. Chem. C* **2021**, *125*, 14065–14074.

[93] E. L. Kunkes, F. Studt, F. Abild-Pedersen, R. Schlögl, M. Behrens, *J. Catal.* **2015**, *328*, 43–48.

[94] S. M. Fehr, K. Nguyen, C. Njel, I. Krossing, *ACS Catal.* **2021**, *11*, 13223–13235.

[95] Y. Wang, S. Kattel, W. Gao, K. Li, P. Liu, J. G. Chen, H. Wang, *Nat. Commun.* **2019**, *10*, 1166.

[96] K. Larmier, W.-C. Liao, S. Tada, E. Lam, R. Verel, A. Bansode, A. Urakawa, A. Comas-Vives, C. Copéret, *Angew. Chem., Int. Ed.* **2017**, *56*, 2318–2323.

[97] T. Fujitani, J. Nakamura, *Appl. Catal., A* **2000**, *191*, 111–129.

[98] A. A. Peterson, F. Abild-Pedersen, F. Studt, J. Rossmeisl, J. K. Nørskov, *Energy Environ. Sci.* **2010**, *3*, 1311.

[99] J. Schaefer, A. Kraft, S. Reininger, G. Santiso-Quinones, D. Himmel, N. Trapp, U. Gellrich, B. Breit, I. Krossing, *Chemistry* **2013**, *19*, 12468–12485.

[100] M. Bowker, *J. Catal.* **1988**, *109*, 263–273.

[101] G. C. Chinchen, P. J. Denny, J. R. Jennings, M. S. Spencer, K. C. Waugh, *Appl. Catal.* **1988**, *36*, 1–65.

[102] X. Wang, H. Zhang, W. Li, *Korean J. Chem. Eng.* **2010**, *27*, 1093–1098.

[103] Y.-F. Shi, P.-L. Kang, C. Shang, Z.-P. Liu, *J. Am. Chem. Soc.* **2022**, *144*, 13401–13414.

[104] M. Zabilskiy, V. L. Sushkevich, D. Palagin, M. A. Newton, F. Krumeich, J. A. van Bokhoven, *Nat. Commun.* **2020**, *11*, 2409.

[105] X.-K. Wu, G.-J. Xia, Z. Huang, D. K. Rai, H. Zhao, J. Zhang, J. Yun, Y.-G. Wang, *Appl. Surf. Sci.* **2020**, *525*, 146481.

[106] M. Behrens, *Angew. Chem., Int. Ed.* **2016**, *55*, 14906–14908.